

# ADAPTIVE METHODS FOR HIGH MACH NUMBER REACTING FLOW

John B. Bell  
Phillip Colella  
John A. Trangenstein  
Michael Welcome

Lawrence Livermore National Laboratory  
Livermore, CA 94550

R. Bell  
A. 2. 4

## Abstract

In this paper we describe some adaptive techniques suitable for modeling high Mach number reacting flows. Two basic types of methods are considered: adaptive mesh techniques and front tracking. Numerical results are described using one of these methods, local mesh refinement, for a simple model for planar detonation. The computational results show the formation of Mach triple points in the detonation fronts and provide an initial step toward understanding the factors influencing the spacing.

## Introduction

Interest in high Mach number reacting flow has increased dramatically in the past few years. In addition to the full gamut of hydrodynamics phenomena, reacting flows also contain small chemical length and time scales corresponding to thin reaction zones in the fluid. The interplay of reactions and hydrodynamic phenomena place far more stringent requirements on numerical methods than are needed for shock hydrodynamics. The numerical difficulties associated with reacting flow are more subtle than just the addition of another sharp front, i.e. the reaction zone, to be represented on the finite difference grid. When conventional shock capturing methods are used to model reacting flow, the interplay between hydrodynamic shock waves and the chemical reactions can lead to spurious, nonphysical waves. For example, it has been shown by Colella, Majda and Rotyburd<sup>1</sup> that if one uses a straightforward capturing method to compute detonations, rather stringent conditions must be placed on the spatial and temporal discretizations. In particular, the mesh spacing and the time step must be chosen so that the internal structure of the detonation is resolved over several time steps. If this conditions is not satisfied, then one can observe unphysical results in the form of spurious weak detonations whose structure and speed are determined purely by the numerical parameters, but which look perfectly reasonable, in that the transitions between the pre- and post-wave states are relatively smooth. It is believed that this phenomena is not peculiar to the particular differencing scheme employed, but would be observed in any conservative finite difference calculation in which the discontinuities were averaged onto a finite difference grid, and for which the time step

was not sufficiently small to resolve the details of the interaction of the energy release with the fluid dynamics.

In light of this example, it is clear that some sort of adaptive strategy will be necessary to calculate high-speed flows with chemistry in more than one space dimension. Since the chemical reaction length and time scales can differ by several orders of magnitude from those of the hydrodynamics the cost of using a uniform grid to resolve the chemical length scales is prohibitive. In this work, we are pursuing two adaptive strategies for dealing with this problem: adaptive mesh techniques, and front tracking.

In the next section we describe each of the adaptive tools in more detail and discuss its role in the overall algorithm. Section three contains the description of a simple, two-step reaction model that we are using as an initial test bed for developing and testing algorithms. Finally, we describe computational results using this model obtained using one of the adaptivity tools; viz., local mesh refinement.

## Adaptive methodologies

### Local mesh refinement

The objective of local mesh refinement is to identify regions within the computational domain where the resolution of the difference scheme is inadequate and to refine the grid within that region. This process can be recursively iterated, defining a multilevel grid structure in which a level  $k$  grid refines over some subset of the level  $k-1$  grids. The hyperbolic character of the basic differential equations, as reflected in the CFL stability restriction of the difference scheme, necessitates a reduction in time step commensurate with the reduction in spatial grid spacing. The approach we are using is one initially developed by Berger and Oliger,<sup>2</sup> and extended by Berger and Colella<sup>3</sup> to the case of time-dependent conservation laws.

Error estimation on a level  $k$  grid is performed by using a coarsened computation on that grid. More precisely, if we denote by  $\Delta x_k$ ,  $\Delta y_k$ , and  $\Delta t_k$  the grid spacing and time step size on the level  $k$  grid and we let  $u_k^n$  represent the collection of grid values on the level  $k$  grid at  $t^n$ , we first take two time steps on the level  $k$  grid to compute  $u_k^{n+2}$ . We then perform a single step on a coarsened grid with  $2\Delta x_k$ ,  $2\Delta y_k$ ,  $2\Delta t_k$  spacing by averaging  $u_k^n$  onto the coarser grid to obtain  $u_{k,c}^{n+2}$ . We then let  $u_{k,c}^{n+2}$  represent the average of  $u_k^{n+2}$  onto the coarsened grid. We then compute

$$e_{ij} = |f(u_{k,c}^{n+2}) - f(u_k^{n+2})|$$

for each grid point  $ij$  in the coarsened grid where  $f$  is some functional of the unknowns that defines quantities of interest to

\* This work was performed under the auspices of the U.S. Department of Energy by the Lawrence Livermore National Laboratory under contract No. W-7405-Eng-48. Partial support under contract No. W-7405-Eng-48 was provided by the Applied Mathematical Sciences Program of the Office of Energy Research and by the Air Force Office of Scientific Research under grant No. AFOSR15870016.

provide the basis for refinement. The values of  $e_{ij}$  are proportional to the local error at  $ij$  (with proportionality constant formally related to the order of accuracy of the underlying numerical method). By defining a target error range  $[e_{\min}, e_{\max}]$  we can determine whether a given grid point is appropriately resolved. If  $e_{ij} > e_{\max}$  then the solution is underresolved and cell  $ij$  is "tagged" for refinement. Alternatively, if  $e_{ij} < e_{\min}$  the solution is overresolved and the cell is "tagged" for derefinement. Once the determination of where refinement is required has been completed, a set of heuristic procedures are then used to define a reasonable collection of logically rectangular grids to be refined. Storage is then allocated for refinement of these grids and initial data is provided for the refined grid from the underlying coarse grid. Similar procedures are used to remove refined grids when they are no longer required.

While local refinement has been described here in terms of a fixed rectangular mesh, there is no reason why it cannot be combined with other adaptive grid techniques, such as moving quadrilateral meshes and component grids. Indeed, these techniques can serve a complementary purpose to the local refinement approach. Quadrilateral and component techniques can be used to adapt the underlying coarse meshes to the global solution or boundary geometry; then these coarse meshes can be refined locally for accuracy.

Front tracking

In front tracking, one attempts to treat discontinuities as internal boundaries in the fluid at which the motion of the front, as well as the jump relations across the front, are imposed explicitly as boundary conditions. The specific approach we are taking is that described in Chern and Colella<sup>4</sup> in which a single distinguished front is tracked, while any other fronts are captured by an underlying conservative finite difference calculation. In addition, we allow the tracked front to move through the finite difference grid, thus enabling us to maintain regularity of the grid, even if the tracked front develops kinks or other large distortions. Front tracking also offers a potential solution to the difficulties discussed in Colella et al.<sup>1</sup> By tracking the front, we eliminate the averaging onto the grid which caused the unphysical results to occur. We shall see that there are some possible difficulties to this approach in more than one space dimension, owing to the substantial small-scale transverse structure generated in the solution by the interaction of the reaction zone and the hydrodynamics. We will discuss this further in the conclusions.

It is certainly possible, and in some circumstances, necessary to combine the front tracking and adaptive mesh approaches. In figure 1 we show an example of the use of such a hybrid in the case of a pure gas-dynamic problem with no chemical reaction. The problem is that of shock reflection from an oblique surface; the combination of the incident shock and Mach stem are tracked as a single entity, with all other discontinuities being captured. In addition, a rectangular region, of fixed shape but moving with the tracked shock, is refined by a factor of 4 in each direction. The fact that the refinement is present in the region of interest enables us to resolve features at a fraction of the computational cost of doing so with a uniform grid everywhere. The tracking of the incident shock, as well as adding to the overall accuracy of the calculation, further improves its efficiency by enabling us to cut off the refined region below the top of the grid. If we had not tracked the incident shock, which is the strongest shock in this problem, considerable numerical noise would have been generated at the point where the incident shock crossed the discontinuity in the mesh, which would have contaminated the solution in the reflection region.

The important features of reaction kinetics from a hydrodynamics perspective are discussed in detail in Strehlow<sup>5</sup> and Shchelkin and Troshin.<sup>6</sup> The basic characterization of the reaction as it affects hydrodynamics can be described in terms of an induction-time model. Fluid passes through the initiating shock wave where it is heated. There is then a delay, referred to in the literature as the induction time, during which free radicals are liberated and intermediate compounds are formed, but which appear relatively quiescent hydrodynamically. At the end of the induction time there is a reaction zone in which the chemical energy associated with the reaction is released.

The induction times, which are experimentally measured as functions of temperature and density, provide a good model for reaction kinetics when actual rate data are unavailable or when the specifics of a particular reaction are unimportant. The induction time model we have used is given in the simplest form possible. The induction time  $\tau$ , which is 1 in the undisturbed fluid, satisfies

$$\frac{d\tau}{dt} = -\alpha(T)$$

where

$$\alpha = \begin{cases} -\bar{\alpha}, & T \geq T_c \\ 0, & T < T_c \end{cases}$$

for a given critical temperature.

The other step of the kinetics model describes the energy release associated with burning of a single species. If we let  $z$  denote the fraction of unburnt fuel, then  $z$  satisfies

$$\frac{dz}{dt} = -K(\tau)z$$

where

$$K(\tau) = \begin{cases} \bar{K}, & \tau \leq 0 \\ 0, & \tau > 0 \end{cases}$$

Taken collectively, this reaction model describes an induction time of  $1/\bar{\alpha}$  after the temperature reaches a specified critical level. At the end of the induction time the energy is released in a linear reaction.

If we combine the reaction kinetics model with the equations we obtain the full description of the model

$$U_t + F_x + G_y = H$$

where

$$U = \begin{pmatrix} \rho \\ \rho u \\ \rho v \\ \rho E \\ \rho z \\ \rho \tau \end{pmatrix}, F = \begin{pmatrix} \rho u \\ \rho u^2 + p \\ \rho uv \\ u(\rho E + p) \\ \rho uz \\ \rho u \tau \end{pmatrix}, G = \begin{pmatrix} \rho v \\ \rho uv \\ \rho v^2 + p \\ v(\rho E + p) \\ \rho vz \\ \rho v \tau \end{pmatrix}, H = \begin{pmatrix} 0 \\ 0 \\ 0 \\ 0 \\ -\rho K z \\ -\rho \alpha \end{pmatrix}$$

The reaction is coupled to the flow through the definition of total energy

$$E = e + \rho \left( \frac{u^2 + v^2}{2} \right) + q \phi$$

Finally, to close the model we use a  $\gamma$ -law ideal gas equation of state,  $p = (\gamma - 1)\rho e$  with  $\gamma = \frac{7}{5}$ . Although considerably simplified, this model includes the majority of physical phenomena needed to address the basic hydrodynamics of detonation, and has been used extensively to model multidimensional detonations in large scale numerical simulations. (See, for example, Guirguis et al.<sup>7</sup>)

## Numerical results

In this section we describe sample results for the model discussed in the previous section using local mesh refinement in conjunction with a second-order Godunov method. All of the computations discussed are directed toward analyzing the cellular structures that arise when an initially one-dimensional detonation profile is perturbed. Our problem geometry is that of a two dimensional channel with planar geometry (figure 2). Initially, the solution consists of single jump discontinuity satisfying the Rankine - Hugoniot relations for a one dimensional detonation front.<sup>8</sup>

$$\begin{aligned} u_1 - u_0 &= W(p_1 - p_0) \\ \frac{1}{\rho_1} - \frac{1}{\rho_0} &= -W^2(p_1 - p_0) \\ e_1 - e_0 &= -\frac{(p_1 + p_0)}{2} \left( \frac{1}{\rho_1} - \frac{1}{\rho_0} \right) - q_0 \\ \tau_1, z_1 &= 0, \tau_0, z_0 = 1 \end{aligned}$$

Here the variables with subscript 0 give the state in front of the detonation wave, and the variables with subscript 1 give the state in back of the detonation wave.  $W$ , the Lagrangian wave speed, is given as function of  $p_1$  and  $(p_0, \rho_0, q_0)$  by solving the Rankine - Hugoniot equations and the equation of state for  $W^2$ :

$$W(p_1, \rho_0, \rho_0, q_0)^2 = \frac{((\gamma+1)p_1 + (\gamma-1)p_0)}{2 \left( \frac{1}{\rho_0} - \frac{(\gamma-1)q_0}{(p_1 - p_0)} \right)}$$

We nondimensionalize the pre-wave pressure and density to  $p_0 = 1$ ,  $\rho_0 = \frac{1}{\gamma}$ , and choose  $u_0 = \frac{-W}{\rho_0}$ , so that the unperturbed wave remains stationary on the grid. We also normalize our energy release parameter  $q_0 = C_q e_0$  and the post-wave pressure  $p_1 = C_p p_{CJ}$ . Here  $p_{CJ}$  is the Chapman - Jouguet pressure, i.e., the unique pressure  $p_{CJ} > p_0$  such that

$$W(p_{CJ}, \rho_0, \rho_0, q_0) = (p_{CJ} \rho_{CJ})^{1/2}$$

With these conventions, it suffices to specify  $C_p$  and  $C_q$  for both states to be uniquely determined. The boundary conditions for the problem are that the top and bottom of the channel are reflecting walls; at the right end, we specify supersonic inflow with the value of  $U$  for the inflow state; and at the left end we specify subsonic outflow, with the Riemann invariant  $R_- = u - \frac{2c}{(\gamma-1)}$  given as  $R_-^{out/inflow} = R_-(u_1, p_1, \rho_1)$ .

Our computational strategy is to use the adaptive mesh refinement technique described above with two or three grid levels, i.e. one or two levels of refinement. In all of the calculations described here, the ratio between coarse and fine grids on successive levels is 1:4 in each direction. In addition to the local truncation error conditions for determining where to refine, we impose the additional constraint that any cells for which the  $z < 10^{-3}$  may not be tagged as requiring refinement at the finest level in the calculation. In this way, we concentrate our computational resources in the region where the interaction of the hydrodynamic waves and the reaction zone is taking place.

The underlying integration scheme is a fractional step version of the second order Godunov method discussed in Colella.<sup>9</sup> This scheme is essentially the same algorithm as that described in Colella and Woodward<sup>10</sup>, except that the parabolic interpolation is replaced by piecewise linear interpolation. The integration of the fluid equations is broken up into three fractional steps:  $L_x^{\Delta t}$  which advances the solution according to

$$\frac{\partial U}{\partial t} + \frac{\partial F}{\partial x} = 0$$

by time  $\Delta t$ ;  $L_y^{\Delta t}$ , which advances the solution according to

$$\frac{\partial U}{\partial t} + \frac{\partial G}{\partial y} = 0$$

by time  $\Delta t$ ; and  $L_c^{\Delta t}$ , which advances the solution

$$\frac{\partial U}{\partial t} = H$$

by time  $\Delta t$ . The steps are combined in a second order Strang - type splitting, with the complete evolution operator  $L^{2\Delta t}$  given by

$$L^{2\Delta t} = L_x^{\Delta t} L_y^{\Delta t} L_c^{\Delta t} L_c^{\Delta t} L_y^{\Delta t} L_x^{\Delta t}$$

The one dimensional gas dynamics steps are solved using the second order Godunov algorithm; the zero-dimensional chemistry step is solved exactly.

If the above calculation is run as described, one obtains after a short time a one - dimensional ZND wave structure : the incoming fluid is shocked to a constant state  $U^*$  via a purely gas-dynamic shock; then at a distance  $-u^*/\alpha$  in back of that initiating shock the energy release begins to take place, with the solution approaching  $U_1$  in back of the reaction zone (figure 3). We refer to the region between the initiating shock and the reaction zone as the induction zone. In order to obtain multidimensional effects, this one dimensional solution must be perturbed with a two-dimensional perturbation. We experimented with several methods for introducing perturbations, and found that the long time behavior of the solution was independent of the method used. In the calculations presented here, the perturbation was introduced via the boundary condition at the supersonic inflow. For a time of length .5, the inflow value of  $\tau$  was increased to to 1.2, in the bottom fourth of the inflow boundary. After time .5, the perturbation was turned off. This perturbation has the effect of increasing the distance between the shock and the reaction zone by 20% in the lower quarter of the channel.

In figure 4, we show a time sequence of results for the channel width  $w=32$ ,  $\bar{K} = 245$ , and  $C_q = 3$ . In addition, for all of the results presented here,  $C_p = 2$  and  $\bar{\alpha} = \bar{K}/10$ . There is only one level of refinement in this calculation, with the grid spacing for the coarsest grid  $\Delta x_{base} = .005$ . In these, and all of the plots shown here, boxes are drawn around the fine grids. The initiating shock front is clearly discerned on the right in both the pressure and entropy contours, while the left boundary of the reaction zone, where the energy release takes place, is delineated by the sharp gradient in the entropy. Four periodic cells can be seen spanning the channel; in addition, the solution exhibits periodicity in time, with a period of about .6. Actually, there are small deviations from periodicity in both space and time, probably due to the fact that the channel width is not exactly an integral number of cells wide.

In figure 5, we show a time sequence of results for the same physical parameters, except that the channel width  $w$  is .04. Since a single cell is approximately .08 wide, and is symmetric about its center and its edge, we expect to see the dynamics of half of one cell in this problem. In this case, we use two levels of grid refinement, with  $\Delta x_{base} = .01$ , so that the grid resolution is the same as in the previous calculation. At time .78, we see a Mach triple point on the initiating shock. The reflected shock extends at a shallow angle downward and away from the triple point, and is reflected off the lower wall. The contact discontinuity, seen as a discontinuity in the entropy, extends up from the triple point at a steep angle, almost vertically. The triple point itself is moving down towards the lower wall. By time .98, the triple point has reflected off the bottom wall, and is propagating up the initiating shock towards the top of the channel. This reflection of the

triple point by the wall corresponds in the multiple cell case to the reflection of a triple point and its mirror image across one of the symmetry lines. At the time when the triple point reflected, the contact discontinuity which had been attached to the triple point detaches from the initiating shock and is carried away by the flow. We actually see three distinct contact discontinuities (one poorly resolved, since it is outside the level 3 grid) propagating downstream. Each of these was formed in this fashion by the reflection of the triple point by one or the other of the walls. At time 1.18, the triple point is again propagating downwards, having reflected from the top wall. At time 1.38, the triple point is nearly at the bottom of the channel, and the configuration is that of time .78. Finally, we show the solution two periods later, at time 2.58. We see that this wave pattern sustains itself as a periodic structure over long times, since the solution seen here is essentially the same wave pattern as occurs at time .78.

One of the questions extensively investigated by experimentalists is that of the dependence of the cellular structure on parameters such as the reaction zone width and energy released. Such parameter studies are easily performed computationally. In figure 6, we show results for the same parameter values as the previous case, except that  $\bar{K} = 490$ , i.e., the induction time is half that of the previous case. We see that the cell size is reduced by half in both dimensions, so that a full cell with two triple points fits exactly across the channel. The temporal period remains unchanged at .6.

In figure 7, we show results for  $w = .04$ ,  $\bar{K} = 245$ , and  $C_q = 6$ , thus setting the chemical energy released to be double that for figure 5, with the other parameters remaining the same. The most obvious change in the solution is a substantial increase in the speed of propagation of the triple point, so that the temporal period is now slightly more than .2. Although the mean width of the induction zone is the same, the variations from that mean are much greater than in the previous cases, with the large distortions in the reaction zone. These distortions are a consequence of the fluid being differentially decelerated by the various shocks in the reaction zone. The distance that a fluid particle can travel in the length of time  $1/\bar{\alpha}$  before it begins to release its chemical energy is a strongly varying function of the number of shocks it encounters and their strengths. For example, the boundary of the long thin tendril of unburned fluid extending into the burned fluid at time .78 coincides on one side with one of the contact discontinuities shed by a reflection of the triple point by the wall. The fluid on the side of the contact discontinuity which has already burned was decelerated by the Mach stem side of the triple point and hence experienced a greater deceleration than that experienced by the fluid which was decelerated by the combination of the incident and reflected shocks. Thus, the latter was able to travel farther before it began to release its chemical energy.

#### Discussion and Conclusions

We have seen in the above calculations some of the possible advantages of using adaptive techniques to compute chemically reacting flows. However, they point up some possible problems in using these techniques. The cellular structures in the detonation front generate variations in the flow field, particularly in the temperature and vorticity due to the shedding of the contact discontinuities, which also carry slip, with length scales on the order of the width of the induction zone. In the calculations given above, we have not attempted to resolve the details of those fluctuations once they leave the reaction zone. One question that needs to be resolved is to what extent the detailed dynamics of these fluctuations effect

the large-scale fluid dynamics. It appears from the computations presented here that the mean velocity of the detonation front is not affected by the cellular structures; otherwise, the entire wave front would have moved off the computational domain. Thus, one alternative is to ignore all the fine structure completely. In that case, the detonation could easily be treated as an infinitely thin front using the front tracking method. However, it seems likely that there will be some circumstances under which these high frequency fluctuations cannot be ignored: high frequency fluctuations in the vorticity have the potential for creating turbulence, and high frequency fluctuations in the temperature can have further dynamic effects through both the fluid dynamics and the chemistry. In that case, a possible route to representing these effects at a reasonable cost would be to couple a front tracking method to a sub-grid scale model, with the tracked front acting as a source of fluctuation densities for the model.

From the point of view of studying the detailed multidimensional structure of high-speed reacting flows, the above calculations represent the most preliminary of efforts. One question which we have not been able to study with our current techniques is the process by which these cellular structures come into existence. The reason for this is that the initial perturbation generates a slight curvature in the initiating shock, which is stationary, and nearly aligned with the grid; such a shock is poorly represented by our capturing method. A natural solution to this problem is to track the initiating shock, and capture the remaining structure with the conservative finite difference method. A second question that is natural to study with these techniques is the interaction of strong acoustic waves with flames as a first step in understanding the transition to detonation. Since flames are diffusively driven, it is necessary to track them, while the acoustic waves can be captured on the finite difference grid. Finally, we intend to expand our capabilities in the area of adaptive grid techniques, particularly in the direction of being able to handle more complicated boundary geometries. This will require us to couple the local refinement and front tracking methods to finite difference methods on general quadrilateral grids. This is essential if we are to be able to study phenomena such as supersonic combustion, where the combustor geometry plays an important role.

#### References

1. P. Colella, A. Majda, and V. Roytburd, "Theoretical and numerical structure for reacting shock waves," *SIAM J. Sci. Stat. Comput.*, vol. 7, pp. 1059-1080, Oct. 1986.
2. M. Berger and J. Olinger, "Adaptive mesh refinement for hyperbolic partial differential equations," *J. Comp. Phys.*, vol. 53, 1984.
3. M. Berger and P. Colella, *Adaptive mesh refinement for shock hydrodynamics*, to appear.
4. I.-L. Chern and P. Colella, *A conservative front tracking method for hyperbolic conservation laws*, to appear.
5. R. A. Strehlow, *Fundamental of Combustion*, International Textbook Company, Scranton, Pennsylvania, 1968.
6. K. I. Shchelkin and Ya. K. Troshin, *Gasdynamics of Combustion*, Mono Book Corp., Baltimore, 1965.
7. R. Guirguis, E. S. Oran, and K. Kailasanath, "Numerical simulations of the cellular structure of detonations in liquid nitromethane--regularity of the cell structure," Memorandum Report 5810, NRL, July 31, 1986.
8. R. Courant and K. O. Friedrichs, *Supersonic Flow and Shock Waves*, Springer-Verlag, New York, 1985.

9. P. Colella, "A multidimensional second-order Godunov scheme for conservation laws," LBL-17023, Lawrence Berkeley Laboratory, May 1984.
10. P. Colella and P. R. Woodward, "The piecewise parabolic method (PPM) for gas dynamical simulations," *J. Comp. Phys.*, vol. 54, pp. 174-201, April 1984.

Figure 2: Geometry and initial conditions for the planar detonation problem.

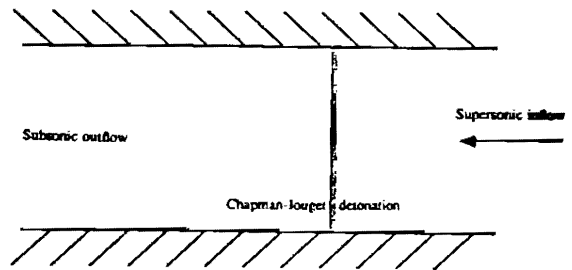


Figure 1: A shock reflection calculation using local refinement and front tracking.

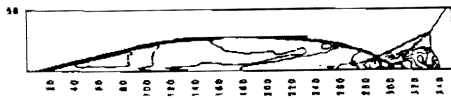


Figure 1a - density plot of the coarse mesh.

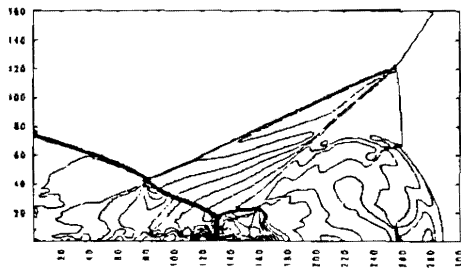


Figure 1b - density plot of the refined region.

Figure 3: Profile of the one-dimensional ZND wave structure.

